

# Emergence of Nonequilibrium Latent Cycles in Unsupervised Generative Modeling

Marco Baiesi<sup>1,2</sup> and Alberto Rosso<sup>3</sup>

<sup>1</sup>*Department of Physics and Astronomy, University of Padova, Via Marzolo 8, I-35131 Padova, Italy*

<sup>2</sup>*INFN, Sezione di Padova, Via Marzolo 8, I-35131 Padova, Italy*

<sup>3</sup>*LPTMS, CNRS, Université Paris-Saclay, 91405, Orsay, France*

We show that nonequilibrium dynamics can play a constructive role in unsupervised machine learning by inducing the spontaneous emergence of latent-state cycles. We introduce a model in which visible and hidden variables interact through two independently parametrized transition matrices, defining a Markov chain whose steady state is intrinsically out of equilibrium. Likelihood maximization drives this system toward nonequilibrium steady states with finite entropy production, reduced self-transition probabilities, and persistent probability currents in the latent space. These cycles are not imposed by the architecture but arise from training, and models that develop them avoid the low-log-likelihood regime associated with nearly reversible dynamics while more faithfully reproducing the empirical distribution of data classes. Compared with equilibrium approaches such as restricted Boltzmann machines, our model breaks the detailed balance between the forward and backward conditional transitions and relies on a log-likelihood gradient that depends explicitly on the last two steps of the Markov chain. Hence, this exploration of the interface between nonequilibrium statistical physics and modern machine learning suggests that introducing irreversibility into latent-variable models can enhance generative performance.

## I. INTRODUCTION

Unsupervised generative modeling aims to learn a probability distribution  $p(\mathbf{x})$  from a dataset  $\mathcal{D}$  of observed configurations [1]. A widespread strategy is to introduce latent variables  $\mathbf{z} \in \mathcal{Z}$  and define a joint distribution  $p(\mathbf{x}, \mathbf{z})$  whose marginal over  $\mathbf{x}$  approximates the data distribution. Classical examples include energy-based models, such as restricted Boltzmann machines (RBMs) [2, 3], where one specifies an energy function  $E(\mathbf{x}, \mathbf{z})$  and sets  $p(\mathbf{x}, \mathbf{z}) \sim e^{-E(\mathbf{x}, \mathbf{z})}$ . In such architectures, the alternation between visible and hidden layers is implemented through Gibbs sampling steps that satisfy a detailed balance. Hence, the learning dynamics is tied to an equilibrium steady state, and the latent-variable transitions are necessarily reversible. While RBMs have been successful in modeling structured data (see, e.g. [4–7]), their reliance on reversible Gibbs updates tends to limit exploration of the configuration space: once a hidden configuration  $\mathbf{z}$  is activated by a given  $\mathbf{x}$ , the sampler typically returns to the same neighborhood [8–10], a behavior reminiscent of slow mixing in equilibrium Monte Carlo methods [11].

Several other classes of latent-variable models have been developed to address limitations of equilibrium generative architectures. Helmholtz machines [12] and deep Boltzmann machines [13] introduced paired “recognition” and “generative” networks, trained, for example, by the wake-sleep phases [12–14], but their sampling dynamics follows a one-way generative path rather than an alternating interaction between visible and latent variables. Modern approaches such as variational autoencoders [15, 16] and diffusion-based generative models [17–22] adopt the same structure: they specify a directed generative process and use a backward inference mechanism to propagate information in the opposite direction. In these frameworks, recognition and generation proceed

along separate pathways, and the latent variables do not participate in a stochastic alternation with the visible layer.

We take a different perspective and propose a generative model whose visible/latent alternation is governed by a generic nonequilibrium Markov chain. We introduce two independently parametrized transition matrices,

$$A_{\mathbf{z}\mathbf{x}} \equiv p(\mathbf{x}|\mathbf{z}), \quad (1)$$

$$\bar{A}_{\mathbf{x}\mathbf{z}} \equiv p(\mathbf{z}|\mathbf{x}), \quad (2)$$

which need not satisfy detailed balance. The composition of these transitions defines a discrete-time Markov process in the bipartite space  $\mathcal{X} \cup \mathcal{Z}$  (see Fig. 1). Because no energy function is available, the stationary distribution has no closed-form expression. Nevertheless, we introduce an approximate log-likelihood gradient that provides a stable and fast-converging training rule.

A central observation of this study is that training a generative model based on generic Markov transitions never selects the reversible, equilibrium limit: the learned dynamics always violates detailed balance. Moreover, the models with the best generative performance operate far

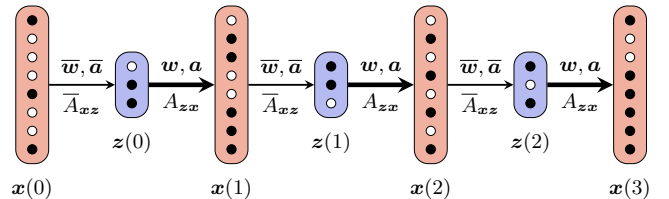


FIG. 1. Markov chain dynamics alternating visible states  $\mathbf{x}(t)$  and hidden  $\mathbf{z}(t)$ . This sequence has  $T = 3$  double steps  $\{\mathbf{x} \rightarrow \mathbf{z} \rightarrow\}$ . The Markov jump probabilities  $\bar{A}_{\mathbf{x}\mathbf{z}}$  of the  $\mathbf{x} \rightarrow \mathbf{z}$  transitions are determined by parameters  $\{\bar{w}, \bar{a}\}$  differing from the parameters  $\{w, a\}$  that govern jump probabilities  $A_{\mathbf{z}\mathbf{x}}$  of the  $\mathbf{z} \rightarrow \mathbf{x}$  transitions.

from equilibrium. To quantify this distance, we study the trajectories of the hidden states through the properties of the Markov matrix

$$M_{z'z} = \sum_{\mathbf{x}} A_{z'\mathbf{x}} \bar{A}_{\mathbf{x}z}, \quad (3)$$

and characterize its behavior in terms of entropy production, persistent probability currents, reduced diagonal occupancy, and long decorrelation times.

Interestingly, likelihood maximization is sufficient to drive the hidden-layer dynamics to self-organize into regular and irreversible cycles. This cyclic behavior is not imposed by the architecture but emerges spontaneously during training as  $M$  develops strong directional flows and long-range temporal structure. Models exhibiting clearer latent-state cycles reproduce more faithfully the empirical distribution of data classes.

These results point to a mechanism through which nonequilibrium dynamics can enhance generative modeling: cycling through hidden states reduces autocorrelation among fantasy samples and encourages a more thorough exploration of the data modes. This suggests that irreversibility may be beneficial not only for sampling, as in nonreversible Monte Carlo methods [23–26], but also for learning itself.

The remainder of the paper introduces the parametrized transition matrices defining the model (Sect. II), derives the associated approximate log-likelihood gradient (Sect. III) and analyzes an example of nonequilibrium steady states that arise during training through entropy production, decorrelation times, and the structure of the latent-to-latent transition matrix (Sect. IV). We end with some conclusions (Sect. V).

## II. MODEL

In this paper, we focus on digital data  $\mathbf{x} = (x_1, \dots, x_D)$  as a  $D$  dimensional array of binary or bit variables  $x_i \in \{0, 1\}$ . Therefore, there are  $2^D$  possible data configurations in the ensemble  $\mathcal{X}$ . Similarly, a hidden variable  $\mathbf{z} = (z_1, \dots, z_L)$  is described by its components  $z_i \in \{0, 1\}$  and has a size  $L \ll D$ .

A state  $\mathbf{z}$  can jump to any of the  $\mathbf{x}$  states via a Markov matrix  $A$ , defined in (1), whose element  $A_{z\mathbf{x}}$  represents the probability of jumping from  $\mathbf{z}$  to  $\mathbf{x}$ . Similarly, a state  $\mathbf{x}$  can transition back to any of the  $\mathbf{z}$  states through a Markov matrix  $\bar{A}$  (Eq. (2)), whose element  $\bar{A}_{\mathbf{x}z}$  gives the probability of jumping from  $\mathbf{x}$  to  $\mathbf{z}$ . In both cases, the conditions

$$\sum_{\mathbf{x} \in \mathcal{X}} A_{z\mathbf{x}} = 1, \quad \forall \mathbf{z}; \quad \sum_{\mathbf{z} \in \mathcal{Z}} \bar{A}_{\mathbf{x}z} = 1, \quad \forall \mathbf{x} \quad (4)$$

ensure the normalization of each row of the Markov matrices. We denote as  $p(\mathbf{x})$  the stationary probability of visible states and as  $\bar{p}(\mathbf{z})$  the stationary probability of hidden states. Given the transition matrices  $A$  and  $\bar{A}$

they satisfy the following equations:

$$p(\mathbf{x}) = \sum_{\mathbf{z} \in \mathcal{Z}} \bar{p}(\mathbf{z}) A_{z\mathbf{x}}, \quad (5)$$

$$\bar{p}(\mathbf{z}) = \sum_{\mathbf{x} \in \mathcal{X}} p(\mathbf{x}) \bar{A}_{\mathbf{x}z}. \quad (6)$$

Following common practice in unsupervised machine learning, we train the model by maximizing the log-likelihood

$$\mathcal{L} = \frac{1}{N_{\mathcal{D}}} \sum_m \ln p(\mathbf{x}) = \langle \ln p(\mathbf{x}) \rangle_{\mathbf{x} \in \mathcal{D}} \quad (7)$$

averaged in the data set  $\mathcal{D} = (x^{(1)}, \dots, x^{(N_{\mathcal{D}})})$ .

The gradient descent to maximize it is performed on the parameters that define the matrices  $A$  and  $\bar{A}$ . For these Markov matrices, we chose the exponential structure typically used for RBMs:

$$A_{z\mathbf{x}} = \frac{e^{\sum_{\alpha,i} x_i w_{i\alpha} z_{\alpha} + \sum_i x_i a_i}}{\sum_{\mathbf{x}'} e^{\sum_{\alpha,i} x'_i w_{i\alpha} z_{\alpha} + \sum_i x'_i a_i}} = \frac{e^{\mathbf{x} \cdot (\mathbf{w} \cdot \mathbf{z} + \mathbf{a})}}{\sum_{\mathbf{x}'} e^{\mathbf{x}' \cdot (\mathbf{w} \cdot \mathbf{z} + \mathbf{a})}}, \quad (8)$$

$$\bar{A}_{\mathbf{x}z} = \frac{e^{\sum_{\alpha,i} z_{\alpha} \bar{w}_{\alpha i} x_i + \sum_{\alpha} z_{\alpha} \bar{a}_{\alpha}}}{\sum_{\mathbf{z}'} e^{\sum_{\alpha,i} z'_{\alpha} \bar{w}_{\alpha i} x_i + \sum_{\alpha} z'_{\alpha} \bar{a}_{\alpha}}} = \frac{e^{\mathbf{z} \cdot (\bar{\mathbf{w}} \cdot \mathbf{x} + \bar{\mathbf{a}})}}{\sum_{\mathbf{z}'} e^{\mathbf{z}' \cdot (\bar{\mathbf{w}} \cdot \mathbf{x} + \bar{\mathbf{a}})}}. \quad (9)$$

Here we denote the local biases for visible and hidden units by  $\mathbf{a}$  and  $\bar{\mathbf{a}}$ , respectively. The weights are given by two separate matrices:  $\mathbf{w}$  of size  $D \times L$  for the transitions  $\mathbf{z} \rightarrow \mathbf{x}$ , and  $\bar{\mathbf{w}}$  of size  $L \times D$  for the transitions  $\mathbf{x} \rightarrow \mathbf{z}$ . Note that, unlike RBMs,  $\mathbf{w}$  and  $\bar{\mathbf{w}}$  are not transposes of each other.

The exponential parameterization of the transition matrices allows for bitwise factorization,

$$A_{z\mathbf{x}} = \prod_{i=1}^D \frac{e^{x_i (\sum_{\alpha} w_{i\alpha} z_{\alpha} + a_i)}}{e^{\sum_{\alpha} w_{i\alpha} z_{\alpha} + a_i} + 1} = \prod_{i=1}^D p(x_i | \mathbf{z}). \quad (10)$$

Similarly, the transition probabilities from  $\mathbf{x}$  to  $\mathbf{z}$  factor as

$$\bar{A}_{\mathbf{x}z} = \prod_{\alpha=1}^L \frac{e^{z_{\alpha} (\sum_i \bar{w}_{\alpha i} x_i + \bar{a}_{\alpha})}}{e^{\sum_i \bar{w}_{\alpha i} x_i + \bar{a}_{\alpha}} + 1} = \prod_{\alpha=1}^L p(z_{\alpha} | \mathbf{x}). \quad (11)$$

These two factorizations enable efficient sampling of the Markov chain: the first equation allows sampling each component  $x_i$  given the hidden state  $\mathbf{z}$ , and the second one allows sampling  $z_{\alpha}$  given  $\mathbf{x}$ .

## III. GRADIENT APPROXIMATION

In principle, we should evaluate the derivatives of  $\ln p(\mathbf{x})$  with respect to the parameters that define the matrices  $\mathbf{w}$ ,  $\bar{\mathbf{w}}$ , and the vectors  $\mathbf{a}$ ,  $\bar{\mathbf{a}}$ , computed on the data points  $\mathbf{x}$ . The stationary distribution  $p(\mathbf{x})$  is the

eigenvector associated with the eigenvalue 1 of the matrix  $\sum_{\mathbf{z}} \bar{A}_{\mathbf{x}', \mathbf{z}} A_{\mathbf{z} \mathbf{x}}$ . However, expressing  $p(\mathbf{x})$  explicitly in terms of parameters and then differentiating it is too complex. We therefore introduce an approximation that restricts the dependence on the parameters to the last two steps of the Markov chain:

$$p(\mathbf{x}) = \sum_{\mathbf{z}} \bar{p}(\mathbf{z}) A_{\mathbf{z} \mathbf{x}} = \sum_{\mathbf{z}} \sum_{\mathbf{x}'} A_{\mathbf{z} \mathbf{x}} \bar{A}_{\mathbf{x}', \mathbf{z}} p(\mathbf{x}'). \quad (12)$$

In particular, the dependence on the parameters that define  $\mathbf{w}$  and  $\mathbf{a}$  is confined to the matrix  $A$  appearing in the second term of the equation, whereas the dependence on  $\bar{\mathbf{w}}$  and  $\bar{\mathbf{a}}$  is limited to the matrix  $\bar{A}$  in the third term. In the next section, we show how the derivatives are evaluated in practice, while in the present section we provide explicit expressions of the derivatives within this approximation.

To compute the derivatives of the log-likelihood  $\mathcal{L}$ , it is useful to first compute the partial derivatives of the two Markov matrices with respect to their parameters,

$$\partial_{w_{j\beta}} A_{\mathbf{z} \mathbf{x}} = A_{\mathbf{z} \mathbf{x}} z_{\beta} (x_j - \mu_{x_j | \mathbf{z}}), \quad (13a)$$

$$\partial_{a_j} A_{\mathbf{z} \mathbf{x}} = A_{\mathbf{z} \mathbf{x}} (x_j - \mu_{x_j | \mathbf{z}}), \quad (13b)$$

$$\partial_{\bar{w}_{\beta j}} \bar{A}_{\mathbf{x} \mathbf{z}} = \bar{A}_{\mathbf{x} \mathbf{z}} x_j (z_{\beta} - \mu_{z_{\beta} | \mathbf{x}}), \quad (13c)$$

$$\partial_{\bar{a}_{\beta}} \bar{A}_{\mathbf{x} \mathbf{z}} = \bar{A}_{\mathbf{x} \mathbf{z}} (z_{\beta} - \mu_{z_{\beta} | \mathbf{x}}), \quad (13d)$$

where  $\mu_{x_j | \mathbf{z}} = \sum_{\mathbf{x}'} x'_j A_{\mathbf{z} \mathbf{x}}$  is the average of component  $j$  of the vector  $\mathbf{x}'$  given  $\mathbf{z}$ ; indeed,  $A_{\mathbf{z} \mathbf{x}'}$  is the conditional probability of  $\mathbf{x}'$  given  $\mathbf{z}$ . Similarly,  $\mu_{z_{\beta} | \mathbf{x}} = \sum_{\mathbf{z}'} z'_{\beta} \bar{A}_{\mathbf{x} \mathbf{z}'}$  is the average of component  $\beta$  of the vectors  $\mathbf{z}'$  given  $\mathbf{x}$ .

Thanks to the factorized exponential structure chosen for the parametrization (see (10) and (11)), these two quantities have simple analytical expressions:

$$\mu_{x_j | \mathbf{z}} = \frac{1}{1 + e^{-(\mathbf{w} \cdot \mathbf{z} + \mathbf{a})_j}}, \quad (14)$$

$$\mu_{z_{\beta} | \mathbf{x}} = \frac{1}{1 + e^{-(\bar{\mathbf{w}} \cdot \mathbf{x} + \bar{\mathbf{a}})_{\beta}}}. \quad (15)$$

Note that (14) depends only on  $\mathbf{z}$ , while (15) depends only on  $\mathbf{x}$ .

The gradient components of a point's log-likelihood  $\ln p(\mathbf{x})$  with respect to  $w_{j\beta}$  or  $a_j$  can be computed using  $p(\mathbf{x}) = \sum_{\mathbf{z}} \bar{p}(\mathbf{z}) A_{\mathbf{z} \mathbf{x}}$ , under the approximation that  $\bar{p}(\mathbf{z})$  is independent of  $w_{j\beta}$  or  $a_j$ . From Eqs. (13a) and (13b) we have

$$\partial_{w_{j\beta}} \ln p(\mathbf{x}) = \frac{\langle A_{\mathbf{z} \mathbf{x}} z_{\beta} (x_j - \mu_{x_j | \mathbf{z}}) \rangle_{\bar{p}(\mathbf{z})}}{\langle A_{\mathbf{z} \mathbf{x}} \rangle_{\bar{p}(\mathbf{z})}}, \quad (16a)$$

$$\partial_{a_j} \ln p(\mathbf{x}) = \frac{\langle A_{\mathbf{z} \mathbf{x}} (x_j - \mu_{x_j | \mathbf{z}}) \rangle_{\bar{p}(\mathbf{z})}}{\langle A_{\mathbf{z} \mathbf{x}} \rangle_{\bar{p}(\mathbf{z})}}, \quad (16b)$$

Here  $\mathbf{x}$  is a given point while  $\langle \cdot \rangle_{\bar{p}(\mathbf{z})}$  denotes the average over the  $\mathbf{z}$  drawn from the model. The same applies to the derivatives with respect to  $\bar{w}_{j\beta}$  or  $\bar{a}_j$ , where one

should use  $p(\mathbf{x}) = \sum_{\mathbf{z}} \sum_{\mathbf{x}'} A_{\mathbf{z} \mathbf{x}} \bar{A}_{\mathbf{x}' \mathbf{z}} p(\mathbf{x}')$ , together with Eqs. (13c) and (13d):

$$\partial_{\bar{w}_{j\beta}} \ln p(\mathbf{x}) = \frac{\langle A_{\mathbf{z} \mathbf{x}} x'_j (z_{\beta} - \mu_{z_{\beta} | \mathbf{x}'}) \rangle_{p(\mathbf{x}', \mathbf{z})}}{\langle A_{\mathbf{z} \mathbf{x}} \rangle_{\bar{p}(\mathbf{z})}} \quad (16c)$$

$$\partial_{\bar{a}_{\beta}} \ln p(\mathbf{x}) = \frac{\langle A_{\mathbf{z} \mathbf{x}} (z_{\beta} - \mu_{z_{\beta} | \mathbf{x}'}) \rangle_{p(\mathbf{x}', \mathbf{z})}}{\langle A_{\mathbf{z} \mathbf{x}} \rangle_{\bar{p}(\mathbf{z})}}. \quad (16d)$$

Here,  $\mathbf{x}$  is a given point, while  $\langle \cdot \rangle_{p(\mathbf{x}', \mathbf{z})}$  denotes the average over  $\mathbf{x}'$  and  $\mathbf{z}$  drawn from the model, with  $p(\mathbf{x}', \mathbf{z}) = p(\mathbf{x}') A_{\mathbf{x}' \mathbf{z}}$ .

To evaluate the approximate gradient, two averages must be taken into account. The first corresponds to the data average over the true samples  $\mathbf{x}$  in (7) applied to the approximate gradient components in (16). This is done by randomly selecting a mini-batch  $\mathcal{N} \subset \mathcal{D}$  of  $N$  data points (with  $N \ll N_{\mathcal{D}}$ ). In practice, this replaces the log-likelihood of full data,  $\mathcal{L}$ , with a stochastic estimate  $\mathcal{L}_{\mathcal{N}}$  [1].

We also adopt the so-called ‘‘centering trick’’ [27], which replaces the data  $\mathbf{x}$  with their deviation from the data average,  $\mathbf{x} - \langle \mathbf{x} \rangle_{\mathbf{x} \in \mathcal{D}}$ , in the exponents of the transition matrix  $\bar{A}_{\mathbf{x} \mathbf{z}}$ . In practice, this modifies the gradient (16c) into

$$\partial_{\bar{w}_{j\beta}} \ln p(\mathbf{x}) = \frac{\langle A_{\mathbf{z} \mathbf{x}}, (\mathbf{x}'_j - \langle \mathbf{x}_j \rangle_{\mathbf{x} \in \mathcal{D}}) (z_{\beta} - \mu_{z_{\beta} | \mathbf{x}'}) \rangle_{p(\mathbf{x}', \mathbf{z}')}}{\langle A_{\mathbf{z} \mathbf{x}} \rangle_{\bar{p}(\mathbf{z})}}. \quad (17)$$

An analogous variant that removes the averages of the hidden variables was not necessary. For RBMs, the centering trick stabilizes learning and makes it independent of the binarization convention (0, 1 or 1, 0). We adopt this trick because we find that it reduces the chance that some hidden units of our model never activate.

The second average is taken over the model distribution, i.e., over the states  $\mathbf{x}'$  and the hidden variables  $\mathbf{z}$  obtained from steady-state sampling of the Markov chain defined by the transition matrices  $A$  and  $\bar{A}$ , as sketched in Fig. 1. In practice, using (10) and (11), we run a Markov chain for  $T$  double steps, producing the sequence

$$\mathcal{T} = [\mathbf{x}'(0), \mathbf{z}(0), \mathbf{x}'(1), \mathbf{z}(1), \dots, \mathbf{x}'(T-1), \mathbf{z}(T-1)]. \quad (18)$$

The prime notation reminds us that these  $\mathbf{x}'$  are ‘‘fantasy particles’’ generated by the model and not true data. To ensure efficient sampling, we employ *persistent contrastive divergence*. The final fantasy state  $\mathbf{x}'(T)$  is reused as the initial state  $\mathbf{x}'(0)$  for the next Markov chain, updated with the new transition matrices. This persistent initialization keeps the chain close to its steady state because the parameters evolve only slowly.

After computing the stochastic gradients of the log-likelihood, we update the transition matrices using a stochastic gradient-ascent step with the RMSprop

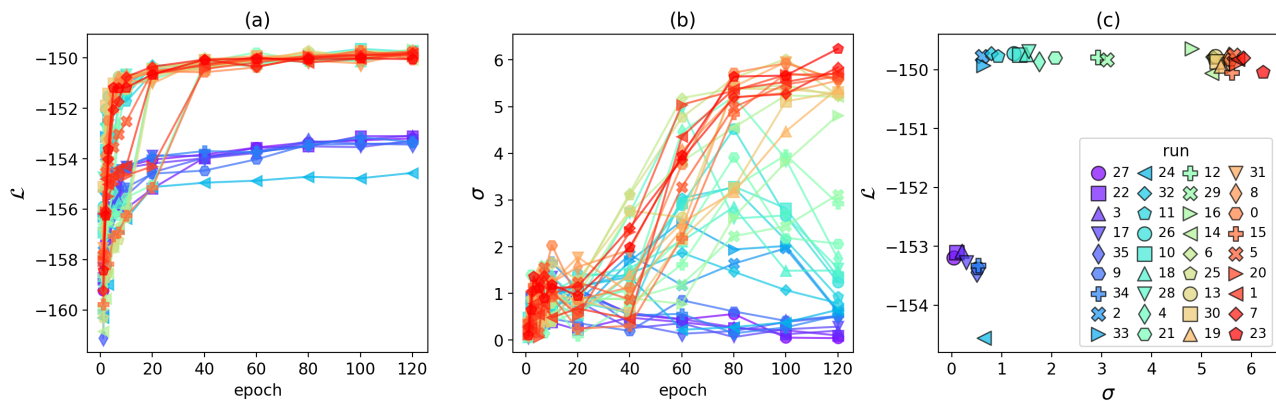


FIG. 2. (a) Log-likelihood as a function the epochs, for the 36 models trained independently. The color code follows the final value of the entropy production rate, shown as a function the epochs in panel (b). Panel (c) shows the log-likelihood vs the  $\sigma$ , at the last epoch of the training.

method, tuned with an appropriate learning rate. A new iteration then restarts with a new mini-batch.

It is important to note that although the gradient is modified by the approximation, the difference vanishes at the maximum of the log-likelihood and we find that it produces stable and reliable training. In other words, both the true and the approximate gradient dynamics converge to the same maximum.

#### IV. EXAMPLE

##### A. Data and parameters

We tested the proposed unsupervised ML method on a selected part of the MNIST dataset of handwritten digits. From such visually interpretable data, we extract the first 1000 instances of the digits, 0, 1, and 2. Hence, the dataset contains  $N_{\mathcal{D}} = 3000$  digits, equally balanced in three classes, and is complex yet small enough for a precise estimate of the log-likelihood. We then digitalize each sample, assigning  $x_i = 1$  to pixels with a gray level above 50% and  $x_i = 0$  otherwise. As a result, our data point  $\mathbf{x}^{(m)}$  is a sequence of  $D = 784$  bits, which can be visualized as an image by reshaping them into a matrix  $28 \times 28$ .

We train a model with  $L = 6$  hidden units, using an RMSprop gradient ascent method with a learning rate  $\eta = 0.1$ . We monitor the learning process by checking the state of the system every 30 gradient ascent steps, a span that we term an *epoch*. During the run, composed of 120 epochs, we schedule the size of the minibatch to increase linearly from  $N = 16$  to  $N = 160$ . In each step, we run a Markov chain with  $T = 48$  steps.

To better monitor the statistics of the hidden states, in this exploratory study, we represent the hidden space  $\mathcal{Z}$  using a one-hot encoding scheme. In this representation, each hidden state  $\mathbf{z}$  is uniquely identified by a single index  $\alpha$  such that  $z_{\alpha} = 1$ , while all other bits are zero.

In the most general formulation, given  $\mathbf{x}$  one must generate the hidden state  $\mathbf{z}$ , a vector of  $L$  binary digits (or bits), whose probability is defined by (11) and factorizes over the individual digits. In particular,  $p(z_{\alpha} = 1|\mathbf{x})$  represents the probability that the digit  $\alpha$  takes the value one. In the one-hot encoding formulation, exactly one  $z_{\alpha} = 1$ , while all the others are zero, and  $\alpha$  is selected with probability

$$p_{\text{one}}(\alpha|\mathbf{x}) = \frac{p(z_{\alpha} = 1|\mathbf{x})}{\sum_{\beta} p(z_{\beta} = 1|\mathbf{x})}. \quad (19)$$

In the following, we use the notation with  $\mathbf{z}$  to emphasize the generality of the results, while we switch to the notation with  $\alpha$ , the single active bit, when appropriate to identify hidden units or entries of the matrices.

In this setting, a visible bias  $\mathbf{a}$  shared by all hidden units is not essential. Indeed, the transformation

$$(w_{i\alpha}, a_i) \longrightarrow (w_{i\alpha} + a_i, 0) \quad (20)$$

leaves unchanged the activation of  $x_i$  due to the hidden unit  $\alpha$ . Since the bias can be fully reabsorbed in the weights, we fix  $\mathbf{a} = 0$  without loss of generality. The initialization of weights is described in the appendix, together with other technical details on stabilization of the code and computation of the log-likelihood.

##### B. Results

Our goal is to understand how the generative performance of the Markov-matrix architecture relates to the dynamical properties of the Markov chain it induces, and in particular to how far its stationary state lies from equilibrium.

As a first measure of generative performance, we monitor the log-likelihood  $\mathcal{L}$  maximized during the training of 36 models (Fig. 2(a)). To characterize the dynamics, we then follow the trajectories of the hidden units  $\mathbf{z}$

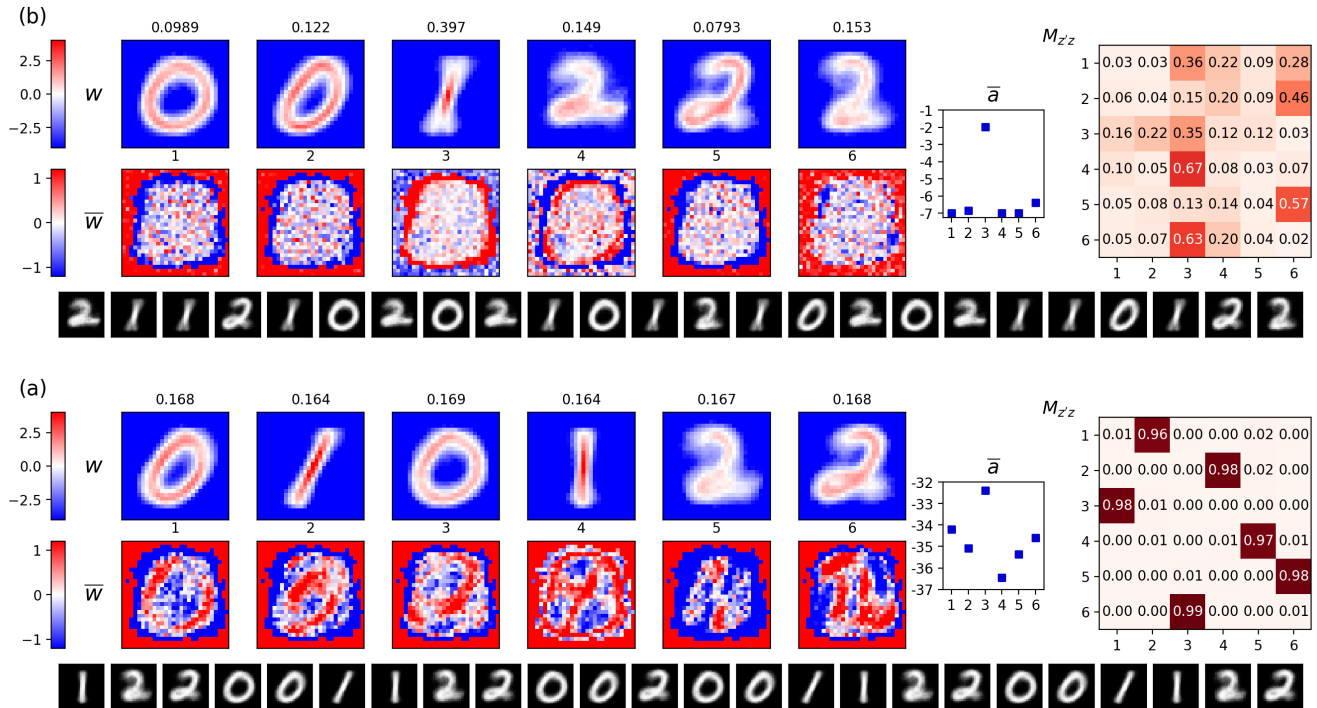


FIG. 3. (a) For run 23, displaying high  $\mathcal{L}$  and  $\sigma$ , plots of the weights  $w_{i\alpha}$  for each of the  $1 \leq \alpha \leq 6$  hidden units (first row,  $D$ -dimensional arrays reshaped to  $28 \times 28$ , with empirical occupancy  $\bar{p}(z = \alpha)$  reported on top), of the corresponding  $\bar{w}_{\alpha i}$  (second row), of the hidden biases  $\bar{a}$  (central panel), of the Markov matrix between  $z$  states (right panel), and a sequence of mean expected states ( $\langle \mathbf{x}(t) \rangle_{z(t-1)}$ , second to last row) and actually generated states ( $\mathbf{x}(t)$ , last row) generated with the Markov chain based on these weights. (b) The same, but for the run 24, displaying low  $\mathcal{L}$  and  $\sigma$ .

and empirically estimate the transition matrix  $M_{z'z}$  of Eq. (3) by counting the transitions on long trajectories and normalizing each row. The stationary distribution  $\bar{p}(z)$  is likewise obtained empirically. As a diagnostic of time-reversal symmetry breaking in the nonequilibrium steady state, we compute the entropy production rate

$$\sigma = \sum_{z' < z} [\bar{p}(z')M_{z'z} - \bar{p}(z)M_{zz'}] \ln \frac{\bar{p}(z')M_{z'z}}{\bar{p}(z)M_{zz'}}. \quad (21)$$

Figure 2(b) shows the evolution of  $\sigma$  during training while Fig. 2(c) shows that, at convergence, the models cluster into three regimes: (i) low  $\mathcal{L}$  and low  $\sigma$ , (ii) high  $\mathcal{L}$  with intermediate  $\sigma$ , and (iii) high  $\mathcal{L}$  with high  $\sigma$ . In particular, low log-likelihood is observed only when the model settles into a nearly reversible regime with small entropy production.

To inspect in detail the features learned by the model, Fig. 3 shows two representative runs: one that reaches both large  $\sigma$  and large  $\mathcal{L}$  (Fig. 3(a)), and one that converges to low values of both quantities (Fig. 3(b)). Each panel displays the learned weights  $\mathbf{w}$ ,  $\bar{\mathbf{w}}$ , and  $\bar{\mathbf{a}}$ , the transition matrix  $M$ , the stationary probabilities  $\bar{p}(z)$  indicated above the  $\mathbf{w}$  panels, and, in the lower row, the average images generated along a sampled sequence of hidden states ( $z(0), z(1), \dots$ ).

In the high-performing run (Fig. 3(a)), each hidden unit encodes a coherent representation of one of the three digits, typically with two distinct variants per digit, and the stationary probabilities  $\bar{p}(z)$  are close to uniform, consistent with the dataset. The transition matrix  $M$  exhibits a dominant off-diagonal entry in each row, leading to strongly irreversible trajectories that cycle through the representations of digits in regular order. In contrast, the run with low  $\mathcal{L}$  and low  $\sigma$  (Fig. 3(b)) displays disordered features: the digit "2" is over-represented by three hidden units, while the digit "1" is only represented by a noisy unit, and the stationary distribution becomes uneven. The transition matrix shows weaker directional structure, hidden states often repeat along sampled trajectories, and the overall dynamics remains closer to reversibility.

To quantify how well the generated samples reproduce the statistics of the dataset, we compute the Kullback–Leibler divergence

$$\text{KL}(P^{\mathcal{D}} \| P^e) = \sum_{k \in \{0,1,2\}} P^{\mathcal{D}}(k) \ln \frac{P^{\mathcal{D}}(k)}{P^e(k)}, \quad (22)$$

where  $P^{\mathcal{D}}(k) = 1/3$  reflects the balanced dataset, and  $P^e(k)$  is obtained by summing  $\bar{p}(z = \alpha)$  over hidden units whose weights  $\mathbf{w}_{\alpha}$  generate digit  $k$ . Figure 4(a)

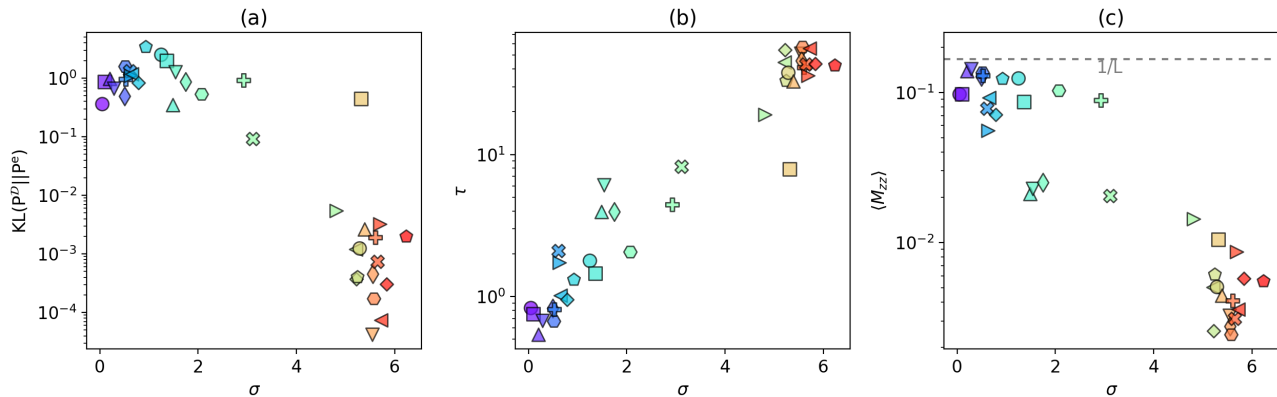


FIG. 4. For the 36 trained models, log-linear plots of several indicators as a function of the entropy production rate: (a) KL divergence between true and empirical distribution of digits; (b) autocorrelation time of  $M_{z'z}$ ; (c) mean diagonal element of  $M_{z'z}$  (it is always lower than the random value  $1/L$ , also for cases with low entropy production rate).

shows that low KL divergence is achieved only for large  $\sigma$ . When  $\sigma$  is small, the generative performance remains poor regardless of the final value of  $\mathcal{L}$ , confirming that nonequilibrium dynamics is essential for accurate sample generation.

We confirm this picture using additional dynamical indicators. First, to quantify the regularity of the dynamics, we compute the decorrelation time

$$\tau = -1/\ln|\lambda_2|, \quad (23)$$

where  $\lambda_2$  is the second-largest eigenvalue (in modulus) of  $M$ . As shown in Fig. 4(b),  $\tau$  correlates strongly with  $\sigma$ : models with large entropy production develop long correlation times ( $\tau \simeq 50$  steps), consistent with nearly deterministic cycles.

To further assess dynamical structure, we examine the mean diagonal element of the transition matrix,

$$\langle M_{zz} \rangle = \frac{\text{Tr}(M)}{L}. \quad (24)$$

Figure 4(c) shows that no trained model exhibits self-transition probabilities that exceed the random baseline  $1/L$ . Even low- $\sigma$  models satisfy  $\langle M_{zz} \rangle < 1/L$ , indicating that training consistently leads to nonequilibrium steady states in which successive hidden states, and consequently the generated fantasy samples, are more decorrelated than in independent random sampling.

Across all models, we find a clear relationship between generative performance and nonequilibrium dynamical properties: high-quality generative behavior arises only in models that develop strongly irreversible, near-cyclic hidden-state dynamics.

## V. CONCLUSIONS

We introduced a generative model in which visible and latent variables interact through two independently

parametrized transition kernels forming a nonequilibrium Markov chain. In comparison with classical RBM equilibrium sampling, this construction breaks the detailed balance between the forward and backward conditional transitions, which leads to qualitatively new behavior. Likelihood maximization drives the system toward nonequilibrium steady states characterized by irreversible probability currents, reduced self-transition probabilities, and the emergence of latent-state cycles.

These cycles are not imposed a priori but arise spontaneously during training. Models that develop a clearer cyclic structure exhibit higher entropy production, longer decorrelation times, and more regular alternation through latent modes. At the same time, they systematically avoid the low log-likelihood regime associated with nearly reversible dynamics and reproduce more faithfully the empirical distribution of classes in the dataset. This suggests that cycling improves the quality of the generative process by decorrelating successive fantasy samples and encouraging a fuller exploration of the data modes.

Our findings bring a nonequilibrium perspective to problems that are usually tackled using equilibrium RBM approaches. Several works focused on understanding and improving the slow sampling caused by the energy landscape that RBMs progressively sculpt during their learning [8–10, 28–30], clarifying the equilibrium and nonequilibrium regimes that arise during learning [31] and the dynamical transitions that can shape training trajectories in energy-based models [32]. These approaches improve the efficiency of Monte Carlo sampling while preserving the detailed balance. In contrast, the mechanism uncovered in this work relies on explicitly breaking reversibility: the most performant models are those whose latent dynamics operates far from equilibrium and organizes into directed cycles.

Recent developments in diffusion-based generative models have highlighted similar connections between

learning, sampling efficiency, and nonequilibrium thermodynamics. In particular, entropy production has been shown to constrain both the speed and accuracy of diffusion model generation [22]. Our findings confirm that nonequilibrium principles can be exploited to design generative models: introducing controlled irreversibility at the latent level can improve exploration and generative performance.

In summary, this work provides a proof of principle that nonequilibrium dynamics can enhance unsupervised generative modeling, even in the minimal setting of a two-layer architecture. The learning rule derived here relies on a log-likelihood gradient that depends on the last two steps of the Markov chain, a structure absent from equilibrium energy-based models. Our results open several directions for future research, including extensions to continuous latent spaces, deeper chains, and a systematic investigation of whether nonequilibrium cycles can provide computational advantages in large-scale generative tasks.

## ACKNOWLEDGMENTS

The authors thank Manjodh Singh, Aurélien Decelle, Beatriz Seoane, and Peter Sollich for the many fruitful discussions. They also thank Marco Boscolo, Francesco La Rovere, Nicolò Montagner, and Raffaele Sabatini for useful discussions on the initialization of weights. M.B. thanks LPTMS in Saclay University and LPTHE in Sorbonne University for the kind hospitality, and LPTMS and CNRS for the support.

## Appendix A: Technical details

### 1. Initialization of weights

The backward weights and biases  $\bar{\mathbf{w}}$  and  $\bar{\mathbf{a}}$  are set to zero so that the hidden states  $\mathbf{z}$  are sampled uniformly during the early stages of learning. For forward weights  $\mathbf{w}$ , we choose an initialization such that a random hidden configuration  $\mathbf{z}$  generates a visible state

$$\mathbf{x} \simeq \langle \mathbf{x} \rangle_{x \in \mathcal{D}},$$

close to the empirical average of the data. In the one-hot encoding scheme for hidden states, the mean activation of a visible unit  $x_i$  follows the logistic expression

$$\langle x_i \rangle_{x \in \mathcal{D}} \simeq \frac{e^{w_{i\alpha}}}{1 + e^{w_{i\alpha}}},$$

Hence, similarly to RBMs' initialization [3], we initialize

$$w_{i\alpha} = \ln \frac{\langle x_i \rangle_{x \in \mathcal{D}(\alpha)}}{1 - \langle x_i \rangle_{x \in \mathcal{D}(\alpha)}},$$

where  $\mathcal{D}(\alpha)$  is a randomly selected subset containing 10% of the dataset. This choice ensures that different hidden units begin learning with slightly different statistical biases, thus promoting differentiation during training.

### 2. Factorized transition probabilities

A numerically more stable variant replaces  $A_{\mathbf{z}\mathbf{x}}$  by

$$A_{\mathbf{z}\mathbf{x}}^* = \prod_{i=1}^D \left[ \frac{e^{x_i(\sum_{\alpha} w_{i\alpha} z_{\alpha} + a_i)}}{e^{\sum_{\alpha} w_{i\alpha} z_{\alpha} + a_i} + 1} Q \right], \quad (\text{A1})$$

where  $Q \approx 1.5$ – $1.8$  compensates for typical sigmoid magnitudes. The ratios  $A_{\mathbf{z}\mathbf{x}}^* / \langle A_{\mathbf{z}\mathbf{x}}^* \rangle_{\bar{p}(\mathbf{z})}$  can then replace  $A_{\mathbf{z}\mathbf{x}} / \langle A_{\mathbf{z}\mathbf{x}} \rangle_{\bar{p}(\mathbf{z})}$  in gradient computations, while the log-likelihoods computed with  $A^*$  include a correction term  $-D \ln Q$ .

For the numerical experiments in the next section, we focus on nonequilibrium steady states with a one-hot latent representation. The corresponding transition probabilities  $\bar{A}_{\mathbf{x}\mathbf{z}}$  are then normalized in a softmax fashion.

### 3. Efficient log-likelihood estimation

A fast on-the-fly estimate of the log-likelihood for a mini-batch  $\mathcal{N}$  is obtained from

$$\mathcal{L}_{\mathcal{N}} \approx \frac{1}{N} \sum_{\mathbf{x} \in \mathcal{N}} \ln \langle A_{\mathbf{z}\mathbf{x}} \rangle_{\mathbf{z}}$$

where the average is over sampled  $\mathbf{z}$  states and time steps  $t$ . A more precise estimate uses long Markov chains (e.g.  $T = 10^5$ ) and all  $N_{\mathcal{D}}$  data points, which requires evaluating  $T \times N_{\mathcal{D}}$  transition probabilities. When the latent space is small, instead one can use the empirical occupancy  $\bar{p}_e(\mathbf{z})$  obtained from the  $T$  Markov samples and compute each  $\ln p(\mathbf{x})$  using (5). This reduces the number of evaluations to  $2^L \times N_{\mathcal{D}}$ , or  $L \times N_{\mathcal{D}}$  for one-hot encoding.

[1] P. Mehta, M. Bukov, C.-H. Wang, A. G. Day, C. Richardson, C. K. Fisher, and D. J. Schwab, A high-bias, low-variance introduction to machine learning for physicists,

Physics Reports **810**, 1 (2019).

[2] P. Smolensky, Information processing in dynamical systems: Foundations of harmony theory (MIT Press, 1986)

Chap. 6.

- [3] G. E. Hinton, A practical guide to training restricted Boltzmann machines, in *Neural Networks: Tricks of the Trade: Second Edition* (Springer, 2012) pp. 599–619.
- [4] C. Malbranke, D. Bikard, S. Cocco, R. Monasson, and J. Tubiana, Machine learning for evolutionary-based and physics-inspired protein design: Current and future synergies, *Current Opinion in Structural Biology* **80**, 102571 (2023).
- [5] J. Fernandez-de Cossio-Diaz, P. Hardouin, F.-X. L. Du Moutier, A. Di Gioacchino, B. Marchand, Y. Ponty, B. Sargueil, R. Monasson, and S. Cocco, Designing molecular RNA switches with restricted Boltzmann machines, *bioRxiv*, 2023 (2023).
- [6] A. Decelle, B. Seoane, and L. Rosset, Unsupervised hierarchical clustering using the learning dynamics of restricted Boltzmann machines, *Physical Review E* **108**, 014110 (2023).
- [7] A. Braghetto, E. Orlandini, and M. Baiesi, Interpretable machine learning of amino acid patterns in proteins: a statistical ensemble approach, *Journal of Chemical Theory and Computation* **19**, 6011 (2023).
- [8] C. Roussel, S. Cocco, and R. Monasson, Barriers and dynamical paths in alternating Gibbs sampling of restricted Boltzmann machines, *Physical Review E* **104**, 034109 (2021).
- [9] E. Agoritsas, G. Catania, A. Decelle, and B. Seoane, Explaining the effects of non-convergent MCMC in the training of energy-based models, in *International Conference on Machine Learning* (PMLR, 2023) pp. 322–336.
- [10] N. Béreux, A. Decelle, C. Furtlehner, L. Rosset, and B. Seoane, Fast training and sampling of restricted Boltzmann machines, in *13th International Conference on Learning Representations-ICLR 2025* (2025).
- [11] M. E. Newman and G. T. Barkema, *Monte Carlo methods in statistical physics* (Clarendon Press, 1999).
- [12] G. E. Hinton, P. Dayan, B. J. Frey, and R. M. Neal, The “wake-sleep” algorithm for unsupervised neural networks, *Science* **268**, 1158 (1995).
- [13] R. Salakhutdinov and G. Hinton, Deep Boltzmann machines, in *Artificial intelligence and statistics* (PMLR, 2009) pp. 448–455.
- [14] J. Bornschein and Y. Bengio, Reweighted wake-sleep, *arXiv preprint arXiv:1406.2751* (2014).
- [15] D. P. Kingma and M. Welling, Auto-encoding variational Bayes, *arXiv preprint arXiv:1312.6114* (2014).
- [16] D. J. Rezende, S. Mohamed, and D. Wierstra, Stochastic backpropagation and approximate inference in deep generative models, in *International conference on machine learning* (PMLR, 2014) pp. 1278–1286.
- [17] J. Sohl-Dickstein, E. Weiss, N. Maheswaranathan, and S. Ganguli, Deep unsupervised learning using nonequilibrium thermodynamics, in *International conference on machine learning* (pmlr, 2015) pp. 2256–2265.
- [18] Y. Song, J. Sohl-Dickstein, D. P. Kingma, A. Kumar, S. Ermon, and B. Poole, Score-based generative modeling through stochastic differential equations, *arXiv preprint arXiv:2011.13456* (2020).
- [19] G. Biroli, T. Bonnaire, V. De Bortoli, and M. Mézard, Dynamical regimes of diffusion models, *Nature Communications* **15**, 9957 (2024).
- [20] M. Kamb and S. Ganguli, An analytic theory of creativity in convolutional diffusion models, *arXiv preprint arXiv:2412.20292* (2024).
- [21] A. Sclocchi, A. Favero, and M. Wyart, A phase transition in diffusion models reveals the hierarchical nature of data, *Proceedings of the National Academy of Sciences* **122**, e2408799121 (2025).
- [22] K. Ikeda, T. Uda, D. Okanohara, and S. Ito, Speed-accuracy relations for diffusion models: Wisdom from nonequilibrium thermodynamics and optimal transport, *Physical Review X* **15**, 031031 (2025).
- [23] P. Diaconis, S. Holmes, and R. M. Neal, Analysis of a nonreversible Markov chain sampler, *Annals of Applied Probability*, 726 (2000).
- [24] E. P. Bernard, W. Krauth, and D. B. Wilson, Event-chain Monte Carlo algorithms for hard-sphere systems, *Physical Review E—Statistical, Nonlinear, and Soft Matter Physics* **80**, 056704 (2009).
- [25] M. Michel, S. C. Kapfer, and W. Krauth, Generalized event-chain Monte Carlo: Constructing rejection-free global-balance algorithms from infinitesimal steps, *The Journal of chemical physics* **140** (2014).
- [26] M. Vucelja, Lifting—a nonreversible Markov chain Monte Carlo algorithm, *American Journal of Physics* **84**, 958 (2016).
- [27] G. Montavon and K.-R. Müller, Deep Boltzmann machines and the centering trick, in *Neural networks: tricks of the trade* (Springer, 2012) pp. 621–637.
- [28] A. Barra, G. Genovese, P. Sollich, and D. Tantari, Phase transitions in restricted Boltzmann machines with generic priors, *Physical Review E* **96**, 042156 (2017).
- [29] J. Tubiana and R. Monasson, Emergence of compositional representations in restricted Boltzmann machines, *Physical Review Letters* **118**, 138301 (2017).
- [30] E. Ventura, S. Cocco, R. Monasson, and F. Zamponi, Unlearning regularization for Boltzmann machines, *Machine Learning: Science and Technology* **5**, 025078 (2024).
- [31] A. Decelle, C. Furtlehner, and B. Seoane, Equilibrium and non-equilibrium regimes in the learning of restricted Boltzmann machines, *Journal of Statistical Mechanics: Theory and Experiment* **2022**, 114009 (2022).
- [32] D. Bachtis, G. Biroli, A. Decelle, and B. Seoane, Cascade of phase transitions in the training of energy-based models, *Advances in neural information processing systems* **37**, 55591 (2024).